GEM TN-93-345

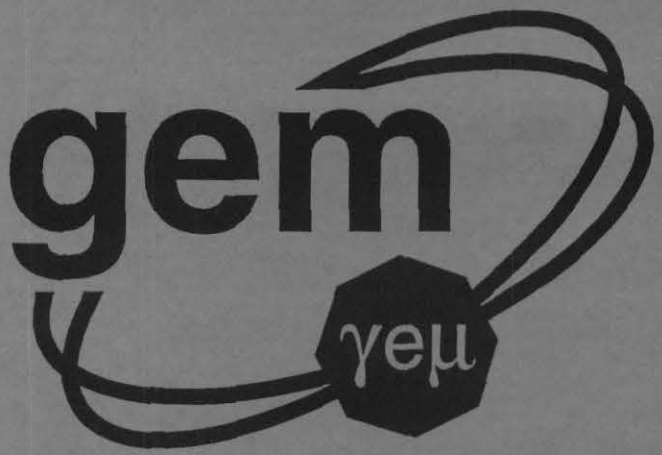

Neutron and Gamma Sensitivity of Gas Detectors

S. Boyarinov, V. Gavrilov, A. Golutvin, R. Kagan, L. Kondratjev, S.Kuleshov,V. Morgunov, F. Ratnikov, V. Rusinov, A.Severenchuck, V.Stolin, I. Tikhomirov, V. Vasilyev

Institute of Theoretical and Experimental Physics

June 14, 1993

Abstract:

Using ^{252}Cf source we have studied the response to fast and thermal neutrons for RDT and CSC filled with different gases. We have also measured the sensitivities of these detectors to gammas from ^{60}Co source.

GEM TN-93-345

June 14, 1993

NEUTRON AND GAMMA SENSITIVITY OF GAS DETECTORS

S.Boyarinov, V.Gavrilov, A.Golutvin, R.Kagan, L.Kondratjev, S.Kuleshov, V.Morgunov, F.Ratnikov, V.Rusinov, A.Severenchuck, V.Stolin, I.Tikhomirov, V.Vasilyev

Institute of Theoretical and Experimental Physics

Abstract

Using ^{252}Cf source we have studied the response to fast and thermal neutrons for RDT and CSC filled with different gases. We have also measured the sensitivities of these detectors to gammas from ^{60}Co source.

Contents

1 Introduction

Muon detectors at future supercolliders will have to operate under environment of substantial neutron and associated gamma fluences (see e.g. [1, 2]). In order to evaluate how this irradiation will affect on muon detector performance (trigger capability and pattern recognition efficiency) occupancy per channel should be estimated:

$$Occupancy = \mathcal{L} \cdot S_{ch} \cdot \Delta\tau \cdot \sum_{n,\gamma} \int dn/dE \cdot \eta(E) dE$$

Here $\mathcal{L}$ is the collider luminosity, S_{ch} is the channel area, $\Delta\tau$ is integration time, dn/dE is neutron/gamma spectrum at the detector position normalized to unit luminosity and $\eta(E)$ is detector sensitivity to neutron/gamma with the energy of E. The study of possibilities to reduce neutron/gamma fluxes in muon detectors is underway. The expected fluencies and energy distributions of neutrons and gammas calculated using various codes [3, 4, 5] agree to each other within a factor of two. However more experimental data still required to check these codes at different set-up conditions.

Fig.1 shows typical spectrum of neutrons passing GEM muon chambers calculated using LAHET-MCNP [3]. The spectrum spans over 8-10 orders of neutron energy and has a thermal peak following flat distribution up to 1 MeV. Therefore in order to estimate the muon chamber rates caused by neutron background one should know the sensitivity to neutrons in a wide energy range.

Neutron associated gammas produced mainly via radiation capture (n, γ) reaction with energies in the range of $0.1 < E_\gamma < 10$ MeV. Due to several rescattering suffered gammas before the entering muon chambers, their spectra at the muon chamber position are estimated to be peaking at the energy about 0.1 MeV [2] (Fig.2).

The results of previous study of limited streamer drift tubes (LSDT) and cathode strip chambers (CSC) sensitivities to neutrons were reported in [6, 7]. The result for CSC was found to be in significant disagreement with simple expectation based on the values of total cross-sections [7]. So the more careful measurements were required.

While measuring the neutron sensitivity of gaseous detectors the following problems should be resolved experimentally:

- the rate due to gammas usually accompaning neutrons should be suppressed and/or subtracted;
- the contribution of neutron and gamma albedo from the floor, walls and other bulk material peaces into detector rate should be suppressed and subtracted as well;
- neutron fluence through detector should be measured by well calibrated neutron detector which is insensitive to gammas.

It should be noted that for the gaseous detectors which are in about ten times more sensitive to gammas with respect to neutrons the first two items require a delicate approach to their solutions.

In order to respond the above problems the ITEP set-up was located at the center of a large concrete box and the minimum amount of material was placed in the vicinity of both the neutron source and the detector. We performed a number of complementary

measurements for different gas detectors. Neutron fluxes at the detector position for various set-up configurations were measured using neutron counter based on $^6Li(n,\alpha)^3H$ reaction which is insensitive to gammas.

2 Experimental Set-up

Two projections of the experimental layout are shown in Fig.3. The set-up includes radioactive source, polyethylene moderator and cadmium absorber (optionally), Pb shielding and tested detector which can be located at various distances from the radioactive source.

2.1 Radioactive sources and neutron flux measurement

As a neutron source we used ^{252}Cf spontaneous fission source with intensity of $\approx 10^7$ neutrons/sec. Bare ^{252}Cf source emits neutrons in the energy range of $0.1 - 10MeV$ peaking near $2MeV$. In order to measure the detector response to the neutrons of thermal energies ($E_n < 0.4eV$) the ^{252}Cf source was placed into a cylinder polyethylene moderator of 18 cm diameter and 20 cm height. The energy spectra of ^{252}Cf neutrons at the detector position have been calculated for various set-up configurations using LAHET-MCNP program [3] which included complete description of experimental set-up. The spectra of neutrons reached the detector acquires a long tail down to thermal energies. In the case of bare ^{252}Cf source about 85% of neutrons have energy higher than 0.1 MeV. The thermal peak contains considerable fractions of neutrons in the set-up containing the moderator (Fig.4). The measurement of detector sensitivity to thermal neutrons ($E_n < 0.4eV$) was achieved with the aid of 1 mm thick cadmium absorber which has a distinctive feature to absorb all neutrons with energies below $\approx 0.4eV$ [8] (Fig.5). Thus we can study the response of the detectors to the fast and thermal neutrons separately.

^{252}Cf source emits factor of 10 more gammas as compare to neutrons. In addition to this gamma flux the neutrons moderated in polyethylene can produce 2.2 MeV gammas via p(n,γ)d reaction. In most of our measurements we protected exposed detectors from gamma radiation with 108 mm thick lead shielding.

The neutron fluxes for all set-up configurations have been measured using all-wave neutron counter MKS-01R which registers α particles produced via $^6Li(n,\alpha)^3H$ reaction on thermal neutrons. Two modifications of this device has been used. The open sensitive element of MKS-01R measures the flux of thermal neutrons. In order to measure the abthermal neutron flux the sensitive element of the counter is inserted inside polyethylene sphere covered by 1 mm thick Cd absorber to provide efficiency roughly independent on neutron energy.

We have paid particular attention to the calibration of MKS-01R counter. The calibration has been performed in precisely monitored neutron fields for fast and thermal neutrons separately. The specially calibrated Pu-Be source was used to provide a flux of neutrons with energies of $\approx 2MeV$ at the position of MKS-01R. The calibrated thermal neutron field was provided by two different ways. Firstly, we used 14-MeV neutron gener-

ator with Pb target and graphite moderator. Secondly, thermal neutron field was created by ^{252}Cf source analogous to our exeriment. Thermal neutron fields were measured by activation of ^{235}U foils for both cases. The efficiency of MKS-01R counter was found to coincide within 15% accuracy for these two measurements. The overall uncertainties of MKS-01R counter calibrations are estimated to be about 20%.

Table 1. Neutron and gamma fluxes $(1/cm^2/sec)$ for ^{252}Cf set-up

Set-up		$E_n > 0.4MeV$		$E_n < 0.4MeV$		γ	
Pb shield	Moder.	36 cm	72 cm	36 cm	72 cm	36 cm	72 cm
–	–	635	200				
+	–	439	132				
		385	*112*	*19*	*21*	*26*	*24*
+	+	160	49	72	24		
		179	*52*	*124*	*43*	*34*	*19*

The measured neutron fluxes for various set-up configurations are listed in Table 1. The calculated values of neutron and gamma fluxes are listed at the bottom of the boxes. The overall normalization of the calculated fluxes were performed using the measured flux of fast neutrons for bare ^{252}Cf source without Pb shielding. Therefore the uncertainty in neutron counter sensitivity to fast neutrons is canceled for comparison of measured and calculated fluxes of fast neutrons whereas for thermal neutrons the uncertainties in calibration of neutron counter sensitivity to both fast and thermal neutrons should be taken into account. Flux of abthermal neutrons from bare ^{252}Cf source with Pb shield have been measured for different distances (R) of the neutron counter from the source (Fig.6). It was found that the flux dependence on R can be approximated as:

$$\Phi(R) = a/R^2 + b$$

The first term corresponds to direct neutron flux from the source while the second one corresponds to albedo neutrons. The fraction of albedo neutrons with $E_n > 0.4$ eV is about 5% at 36 cm distance from the source. This value is in a good agreement with neutron flux calculations performed for actual set-up configuration and for "ideal" set-up without taking into account walls, floor and ceiling.

As a source of gammas we used the ^{60}Co. This source has an intensity of $\approx 10^6$ gammas per second and emits two gamma lines with energies 1.17 and 1.33 MeV. The gamma fluxes at different distances from the source were just calculated on the base of ^{60}Co intensity provided in its specification.

2.2 Detectors

We studied neutron and gamma sensitivity for two options of gas detectors considered for muon system, namely, RDT and CSC filled with various gas mixtures. The parameters of RDTs detectors are shown in Table 2.

Table 2. Parameters of RDTs

Code	RDT1	RDT2	RDT3
Wall material	Fe	Al	Mylar
Inner diameter,mm	18	26.5	26
Wall thickness, mm	1.0	0.7	0.07 Mylar 0.005 Al
Length,mm	142	180	196

It also should be noted that Fe RDT was originally designed to operate under the high gas pressure and it has been assembled with three 1 cm diameter copper rods to reinforce the chamber endcaps. One gap CSC prototype with sensitive area 160×110 mm have been assembled of 1.5 mm thick G10 plates with $80\mu m$ thick Cu cathodes and 25 mm thick Hexel panel at the front of CSC. Gas gap of CSC was 5 mm thick. All RDTs and CSC detectors were operated in proportional mode with gas gain of about $few \times 10^4$. The charge collected at the anode was integrated within 1.4 μs gate and digitized by ADC. The calibration of ADC scale as well as the gas gain measurements have been performed for each detector and operating gas using ^{55}Fe source. The threshold of hit registration was set to be about of 0.5 keV of electron energy loss in the sensitive gas volume.

2.3 Albedo subtraction and gamma mitigation

In order to measure the contribution of albedo neutrons and gammas into detector rate the measurements for different distances from sources to detectors have been performed. Fig.7 shows typical dependencies of detector rate vs $1/R^2$ where R is the distance between the source and the detector. Similar to the neutron flux they were approximated by the function

$$r(R) = a/R^2 + b$$

In the case of ^{252}Cf source the fraction of albedo neutrons (both thermal and abthermal) in the total neutron fluence through detector is of the order of 10% for 36 cm distance between source and detector. However the contribution of albedo particles into detector rate at this distance is higher. The reason is much higher sensitivity of our gas detectors to gammas with respect to neutrons. Taking into account the calculated flux of albedo gammas (Table 1) and ratio of the measured detector sensitivities to neutrons and gammas albedo level in Fig.7a can be explained. In the case of ^{60}Co gamma source the relative contribution of albedo gammas to detector rate is significantly lower (Fig.7b).

In order to subtract albedo contribution from the measured detector rate all measurements have been performed for two distances between sources and detectors (namely 36 and 72 cm) and direct rate was calculated as follows:

$$N_{dir}(36) = 4/3[N_{det}(36) - N_{det}(72)]$$

As was mentioned ^{252}Cf source emits more gammas than neutrons. In order to decrease this direct gamma flux as well as flux of gammas emitted in $p(n,\gamma)d$ reaction in

moderator through detector we used pure Pb sheets placed between source (moderator) and detector as shown in fig.3. The optimal thickness of this Pb shield was found by measurement of detector rate corrected to albedo as a function of Pb shield thickness (Fig.8). This dependence can be approximated by the sum of two exponentials corresponding to gamma and neutron absorption in lead. The slope corresponding to neutron absorption is in a good agreement with direct measurement of neutron flux attenuation by 108 mm thick of Pb. We used 108 mm thick Pb shield for all measurements of neutron sensitivities. For such a shield the contribution of direct gammas emitted by the source into detector rate is of the order of 10% or less depending on detector and gas. Some gammas are produced at neutron capture by lead nuclei. There is equilibrium value of gammas/neutron fluxes ratio if the thickness of Pb shield is large enough. By the way this ratio is expected to be about few % for pure lead that we used in our experiment.

3 Results

3.1 Sensitivity to fast neutrons

The sensitivities of studied detectors to fast neutrons have been measured for bare ^{252}Cf spectrum. The response of detectors to fast neutrons ($E_n > 0.1MeV$) have been found after the subtraction of the albedo rate:

$$\eta = \frac{N_{det}(36) - N_{det}(72)}{S \cdot [\Phi(36) - \Phi(72)]}$$

where $N_{det}(R)$ and $\Phi(R)$ are measured detector rates and fast neutron fluxes, S is transversal cross-section of sensitive detector volume.

Table 3 summarizes the sensitivities of detectors to fast neutrons.

Table 3. Sensitivities of gas detectors to fast neutrons (in units of 10^{-3})

Gas	iC_4H_{10}/Ar				
iC_4H_{10} fraction	100%	100%	20%	100%	90%
Detector	RDT1	RDT2		RDT3	LSDT
η_{det}	1.7	1.8	0.57	1.6	3.1
η_{cm}	1.2	0.87	0.27	0.78	1.4
η_{el}	1.0	1.0	0.22	1.0	0.9

Gas	CF_4			
Detector	RDT1	RDT2	RDT3	CSC
η_{det}	0.67	0.65	0.80	0.20
η_{cm}	0.47	0.31	0.39	0.40
η_{el}	0.25±0.1			

Statistical errors of these results are negligible. The long term reproducibility of the results of the measurements was better than 10%. So the systematic errors caused by an uncertainty in the distance from the source to the detector, uncertainties in the threshold, gas purity and pressure are estimated to be not higher than 10%. The systematic error in the absolute values of measured sensitivities caused by the uncertainty in the neutron counter calibration is about 20%. It should be noted that the detector rate caused by neutrons and gammas reflected or emitted by the material located at the vicinity of the detector (e.g. RDT support and movable platform under detector) was not subtracted using our method of albedo subtraction. However the flux of these neutrons was partially taken into account using neutron counter measurements for the same environment, but the gammas lead to some overestimation of measured detector sensitivity to fast neutrons (especially in the case of Fe RDT).

For the sake of comparison of data for different detectors the values of detector sensitivities per 1 cm of neutron path length in sensitive gas volume are listed in Table 3 also. Reasonable agreement between data for the same gases can be noted. Sensitivities of iC_4H_{10} filled detectors to fast neutrons are higher than for CF_4 because of high density of hydrogen nuclei for the former gas.

The effect of an unsubtracted gamma background in the measured sensitivity to fast neutrons was studied by variation of the fraction of iC_4H_{10} in iC_4H_{10}/Ar mixture filling the detector. Because of the probability of neutron elastic scattering on nuclei for Ar monoatomic gas is much less than that for iC_4H_{10} and additionally the energy of Ar recoil nuclei is also considerably lower than that for H and even C nuclei, the sensitivity to fast neutrons of gas detectors filled with Ar is expected to be much lower than for iC_4H_{10}. Fig.9 shows the sensitivity of Al RDT to fast neutrons measured using described above method as a function of volume fraction of iC_4H_{10} in iC_4H_{10}/Ar mixture. This dependence can be approximated by linear function. The value of the intersept at zero percentage of iC_4H_{10} is about $3 \cdot 10^{-4}$ which seems to be in 3-5 times higher than the estimated probability of nAr elastic scattering with energy transfer higher than the threshold of gas ionization. Therefore this value allow to estimate qualitatively the value of the unsubtracted contribution of gamma background in measured sensitivities to fast neutrons listed in Table 3. Quantitative analysis of such contribution require knowledge of gamma spectra because of the probability of gamma absorption via photoeffect on gas atoms depends strongly on gas content whereas detection of electrons from Compton scattering in the detector walls does not depend on the gas.

The LSDT sensitivity to fast neutrons (for the similar bare ^{252}Cf spectrum) was measured at MIT [6]. The value of "gas alone efficiency" of LSDT found using a similar measurement of neutron sensitivity vs iC_4H_{10} content in iC_4H_{10}/Ar mixture is quoted in Table 3. This result is in good agreement with our data.

The sensitivity of gas detector to fast neutrons due to elastic scattering off gas nuclei can be estimated using the following expression:

$$\eta_{el} = N_a < l > \sum_A n_A \int \frac{dN}{dE_n} \sigma_{nA}^{el}(E_n) \left(1 - \frac{E_{thr}(A)}{E_{max}(A, E_n)}\right) dE_n$$

where N_a is the number of molecules in 1 cm^3 of gas at normal pressure, $< l >$ is the average neutron path length in sensitive gas volume, n_A is the number of atoms of mass

A in the gas molecule times volume fraction of this gas content, dN/dE_n is the neutron spectrum normalized to one neutron, σ^{el}_{nA} is cross-section of nA elastic scattering, E_{thr} is the minimum recoil energy required for gas ionization, $E_{max} = 4AE_n/(A+1)^2$ is the maximum energy transferred from neutron with energy of E_n to the nucleus at elastic scattering. The values of η_{el} calculated for $< l >= 1cm$ on the base of elastic cross-sections from [8] and E_{thr} estimated using results of [9] are listed in the last line of table 3. The uncertainties in these values comes mainly from the uncertainty in E_{thr} are estimated to be about 10% for iC_4H_{10}/Ar mixtures and $\approx$ 40% for CF_4. Taking into account the uncertainties in both experimental data ($\approx$ 20%) and calculations the agreement between data and calculated values is observed for the different gas detectors listed in Table 3. This justifies the assumption that in the energy range from 0.1 to 10 MeV the main mechanism of neutron detection in tested detectors is the elastic scattering of neutrons on gas nuclei and consequent gas ionization by recoil atoms or ions.

The result of the measurement of CSC sensitivity to fast neutrons mentioned in [7] is in 20 times higher than the corresponding value of η_{el}. However there are at least two reasons that can help to explain why the value of neutron sensitivity quoted in [7] was considerably overestimated:

- The neutron flux at the detector position behind Pb shield have not been measured for data of [7]. Instead the detector rate attributed to neutrons was extrapolated to zero thickness of Pb. However the attenuation coefficient (found in [7] on the base of measurements for Pb shield thickness variation up to 100 mm) was significantly higher than measured here for wider Pb thickness range (up to 180 mm, see Fig.8) and independently checked using neutron counter measurements with and without Pb shield. Using the attenuation coefficient determined in our study and the measured CSC rate for 100mm thick Pb shield from [7] one can find that CSC rate extrapolated to zero Pb thickness is more than 2 times lower than used in [7] for neutron sensitivity determination.

- The background of albedo neutrons and gammas have not been measured or estimated for data of [7]. However the measurements performed for LSDT [6] at almost the same experimental environment as for the measurements of [7] indicated to the considerable gamma background even with respect to neutron sensitivity of LSDT filled with iC_4H_{10}. In the case of CSC filled with CF_4/CO_2 mixture the fraction of gamma background rate is expected to be higher due to smaller gas gap of CSC with respect to LSDT and lower sensitivity to fast neutrons of detector filled with CF_4/CO_2 mixture with respect to iC_4H_{10}.

Fig.10a shows the distribution of the collected charge for mylar RDT filled with CF_4 for fast neutron detection after the subtraction of albedo contribution. The same data presented in the integrated form as a probability of neutron detection versus the threshold of the collected charge are shown in Fig.10b. One can see the considerable fraction of hits with the collected charge much higher than that of one minimum ionizing particle (MIP) (1 MIP $\simeq$ 5 keV in 1 cm of CF_4). Data of Fig.10 are in a qualitative agreement with the energy distribution of recoil nuclei for neutron elastic scattering. Quantitative comparison will require accurate description of gas ionization by low energy heavy ions,

of subsequent recombination at high density ionization and of gas gain in the case of high density primary ionization.

3.2 Sensitivity to thermal neutrons

In case of thermal neutrons the main mechanism of thier registration by gas detectors is completely different with respect to fast neutrons. For thermal neutrons the elastic scattering off gas nuclei is not lead to any gas ionization, but cross-sections of radiation neutron capture are much higher for many of the nuclei with respect that for fast nuclei [8]. So for thermal neutrons detector response is mainly due to registration of gammas produced in $(n\gamma)$ reactions taking place in detector walls, support structure and other environment. Typically such reactions result in several $(1 \div 4)$ gammas with energies from 100 keV to 10 MeV. The set of these energies is different for different nuclei. These gammas in turn should generate electrons (or pairs) which will give ionization in sensitive volume. Pair production provide sizable contribution only for gamma energies higher than 5 MeV so this mechanism does not play significant role in thermal neutron detection because of the fraction of gammas with required energies is small. The Compton scattering in gas, detector walls and in material outside detector (provided the transferred to electron energy will allow it to penetrate detector wall) seems to be the main mechanism of thermal neutron detection in our case. The electron knock-out via photoeffect on gas atom provides some contribution into thermal neutron sensitivity also. The role of the last mechanism increases for thin wall detectors and for high Z gases.

As was mentioned above the polyethylene moderator and Cd absorber were used to measure sensitivities of gas detectors to thermal neutrons. Because of transparency of 1 mm Cd foil changes very rapidly from $\approx 10^{-5}$ at $E_n \leq 0.25eV$ to 0.9 at $E_n = 1eV$ and 0.98 at $E_n \geq 10eV$ [8] using Cd foil in combination with polyethylene moderator (see Fig.3b) allows to measure detector response to neutrons from thermal energy region separately from abthermal region. The values of sensitivities were calculated as follows:

$$\eta_{th} = \frac{N_m(36) - N_m(72) - N_{m/Cd}(36) + N_{m/Cd}(72)}{S \cdot [\Phi_{th}(36) - \Phi_{th}(72)]}$$

Here $N_m(R)$ and $N_{m/Cd}(R)$ are detector rates for set-up configuration with moderator without or with Cd absorber correspondently, $\Phi_{th}(R)$ is the thermal neutron flux for set up with moderator and without Cd absorber. The measured values of sensitivities to thermal neutrons are listed in table 4.

Table 4. Sensitivities of detectors to thermal neutrons (in units of 10^{-3})

Gas	iC_4H_{10}		CF_4		
Detector	RDT2	RDT3	RDT2	RDT3	CSC
Sensitivity	1.2	2.0	1.8	3.0	0.65

The following regularities can be noted for this data:

- In contrast to the case of fast neutrons the sensitivity to thermal neutrons is slightly

higher for CF_4 gas with respect to iC_4H_{10}. A possible explanation of it may be the larger cross-section of photoeffect for F nuclei with respect to C.

- The sensitivity of mylar RDT to thermal neutrons is higher with respect to Al RDT. The reason is that mylar walls are much more transparent for low energy photons and electrons with respect to Al walls. This observation shows the significant role of environment in the thermal neutron detection (especially for thin wall detectors).

- Similar to the case of fast neutrons the sensitivity of CSC to thermal neutrons is significantly lower with respect to RDT. However if for fast neutrons the reason was simply smaller gas gap of CSC, for the thermal neutrons the explanation looks to be different. Namely, the Hexel panel and G10 plates shield CSC gas gap against external electrons and the copper cathodes shield it against low energy photons. In addition the fraction of support material at out set-up was smaller for CSC with respect to RDT.

The measured sensitivities of RDTs to thermal neutrons are significantly higher than we estimated taking into account only detector material. It indicates once more to the significant role of environment. It is clear that for muon detectors at supercolliders the environment will be significantly different than that for our set-up. From one hand we have some auxiliary supports and movable platform, but from another hand the full scale muon detectors will consist of large size multilayer chambers. So in order to estimate more accurate a sensitivity to thermal neutrons for actual muon detector the measurements for large multilayer prototypes will be required.

Fig.11a shows the distribution of the collected charge for mylar RDT filled by CF_4 for thermal neutron detection. The same data presented in the integrated form as a probability of neutron detection versus threshold of collected charge are shown in Fig.11b. It can be noted that in the case of thermal neutrons the tail of this distribution is shorter with respect to fast neutrons but it is longer with respect to minimum ionizing particle passing through RDT in the direction normal to the anode wire. The last feature can be explained by a wide angular distribution of electrons penetrating RDT for thermal neutron case.

3.3 Radioactivation

Radioactivation of muon detector material by neutrons also lead to background rate. The thermal neutrons provide the major contribution in radioactivation because the neutron capture cross-sections decrease very rapidly with neutron energy increase. We have measured such rates for Al RDT and CSC. For this purpose we irradiated the detectors by neutrons of moderated spectrum during one hour. The neutron fluxes through the detectors were measured to be: $5 \cdot 10^3 sec^{-1}$ p for RDT and $1.7 \cdot 10^4 sec^{-1}$ for CSC. After removing the neutron source we measured the detector rates as a function of time period after irradiation (see Fig.12). The beta decay components for ^{28}Al ($T_{1/2} = 2.3$ min) and ^{66}Cu ($T_{1/2} = 5.1$ min) are clearly seen. The approximation of the data by exponential function plus constant provides the following values of equilibrium detector rates due to the beta decays: $(3.3 \pm 0.5) Hz$ for Al RDT and $(1.4 \pm 0.3) Hz$ for CSC. The rates normalized to the neutron fluxes are listed in Table 5 (W_β^{exp}).

Table5. Probability of β-decay detection per one thermal neutron

Detector	Isotope	E_β^{max} (MeV)	$T_{1/2}$	W_β^{exp}	W_β^{calc}
Al RDT	^{28}Al	2.9	2.3 min	$(6.6 \pm 1.)10^{-4}$	$5.6 \cdot 10^{-4}$
CSC	^{66}Cu	2.6	5.1 min	$(8. \pm 2.)10^{-5}$	$5. \cdot 10^{-5}$
	^{64}Cu	0.6	12.8 h	-	$2.2 \cdot 10^{-4}$

The experimental results can be compared with the numbers calculated using the simple expression:

$$W_\beta^{calc} = n_A \cdot \sigma_{th} \cdot < l > \cdot r_\omega$$

where n_A is the number of nuclei of activated isotope per one cm^3, σ_{th} is cross-section of its radioactivation by thermal neutrons, $< l >$ is the average neutron path length in Al or Cu, $r_\omega \approx 0.5$ is the probability of beta ray emission into sensitive gas volume of the detectors. A good agreement between measured and calculated values is observed.

It should be noted that in the case of Cu both the ^{64}Cu and ^{66}Cu isotopes are activated. The half-life time of ^{64}Cu is 12.8 hours and it contributes to constant background in Fig.9b. But the total equilibrium rate of CSC caused by copper radioactivation by thermal neutrons expected to be in 5 times higher than that corresponding to activation of ^{66}Cu isotope only (see Table 5). Comparing the results listed in Tables 4 and 5 one can conclude that the measured sensitivities of both Al RDT and CSC to thermal neutrons is in several times higher than the contribution of beta radioactivation of Al or Cu.

3.4 Results on gammas

The expected spectrum of background photons associated with neutrons for GEM barrel muon chambers [2] calculated using GEANT-CALOR package [4, 5] was shown in Fig.2. This spectrum is softer than summary gamma spectrum from neutron radiative capture because of the gammas suffer a number of rescatterings before reaching the muon chambers and loss considerable fraction of their primary energy.

In the contrast to calculation of sensitivities to neutrons that required a detailed knowledge of all material composition and of neutron cross-sections for a lot of isotops as well as the detailed description of gas ionization by low energy atoms and ions, the sensitivity of gas detectors to photons can be calculated much more reliably just using GEANT simulations. The results of GEANT simulation of photon sensitivity as a function of energy for 6-layer GEM barrel CSC [2] with 5 mm gas gap in 0.8 Tl magnetic field are listed in table 5. GEANT cuts for minimum electron and photon energies were set as low as 10 keV.

Table 5. Results of GEANT simulation of photon sensitivity of GEM barrel CSC

E_γ (MeV)	0.5	1.0	3.0	5.0
$W1$	$1.8 \cdot 10^{-3}$	$5.0 \cdot 10^{-3}$	$1.3 \cdot 10^{-2}$	$1.5 \cdot 10^{-2}$
$W2$	$2.4 \cdot 10^{-6}$	$7.5 \cdot 10^{-6}$	$6.3 \cdot 10^{-5}$	$1.7 \cdot 10^{-4}$

In this table $W1$ means the probability to have hit (ionization) in one of six layers of CSC divided by 6 in the sake of normalization per single layer, $W2$ means the probability to have in any two different layers hits generated by the same photon (double Compton scattering) divided by 15 (number of two layer combinations). It should be noted that the single electron with the energy less than 3 MeV cannot cause hits in two layers because of 2 cm interlayer separation and magnetic field. The results of MC simulations shows that:

- CSC sensitivity to photons is expected to depend strongly on the photon energy.
- CSC sensitivity to photons is expected to be in about 10 times higher than sensitivity to neutrons.
- The double hit probability is expected to be slightly lower than the square of the single hit probability for the photon of the same energy. This is not surprising as far as photon losses part of its energy at the first scattering and the probability of the second one is lower.

In order to check the GEANT simulation of photon sensitivities we performed measurements for ^{60}Co source. The results are presented in Table 6.

Table 6. Sensitivities of gas detectors to gammas from ^{60}Co source (in units of 10^{-3})

Gas	iC_4H_{10}			CF_4			
Detector	RDT1	RDT2	RDT3	RDT1	RDT2	RDT3	CSC
Sensitivity	7.9	8.3	5.9	10.7	11.3	8.9	4.3
MC results		6.8			6.9	1.3	6.7

Table 6 also presents results of GEANT simulations (with 10 keV thresholds) of the detector sensitivities. The material located outside detectors was not taken into account. According to GEANT simulation the Compton scattering of ^{60}Co gammas on electrons in RDT gas volume has the probability $\approx 3 \cdot 10^{-4}$.

Similar to the thermal neutron case the measured sensitivity to gammas seems to be slightly higher for CF_4 gas than for iC_4H_{10}. The reason can be the same: higher probability of photoeffect at the former gas. This feature does not reproduced in GEANT simulation because of the photoeffect is significant for gammas with energies less than about 100 keV that are produced in the material surrounding detector and are not taken into account in the present simulations. Such low energy gammas as well as low energy electron knocked out by primary Co gammas from detector environment are most effective in the case of thin wall mylar RDT whereas direct Compton scattering in this RDT wall

has a low probability. This can explain significant disagreement between experimental results and MC simulation for mylar RDT.

4 Summary

The sensitivities of RDT filled with various gases and of CSC filled with CF_4 to fast and thermal neutrons have been measured using ^{252}Cf neutron fission source. The measurements for different distances between the source and the detectors were used for albedo neutrons and gammas subtraction. 108 mm thick Pb shield was used for mitigation of direct gammas emitted by Cf source. The combination of polyethylene moderator and Cd cover was used for measurement of detector response to thermal neutrons.

The neutron fluxes for each set-up configurations were measured using well calibrated neutron counter operated in two modes: sensitive to thermal or abthermal neutrons. The measured neutron fluxes seems to be in a reasonable agreement with LAHET-MCNP simulations for various set-up configurations.

The sensitivity of all tested detectors to fast neutrons (bare ^{252}Cf spectrum) depends on gas content and is proportional to neutron path length in sensitive gas volume. This means that the gas ionization by recoil atoms or ions at the result of elastic neutron-nucleus scattering is the main mechanism of detection of neutrons with energies from 0.1 up to 10 MeV in the tested detectors. The measured values of sensitivities to fast neutrons are in a good agreement with simple calculations based on neutron elastic cross-sections and kinematics. This means that sensitivity of muon detectors designed for supercolliders to fast neutrons can be relyably estimated by this way. The distribution of fast neutron detection events on the charge collected at the anode has a very long tail up to the values in two orders of magnitude higher than average collected charge for MIP.

The interpretation of gas detectors sensitivities to thermal neutrons is more complicated because the following chain of reactions is involved into detection mechanism: neutron capture, gamma emission and possible rescattering, Compton scattering or photoeffect. Some of the stages of this process can take place in detector walls and surrounding material. For quantitative description of the results for thermal neutrons detailed simulations are required. However the measured values of Al RDT and CSC sensitivities to thermal neutrons (which are slightly higher than sensitivities of the same detectors to fast neutrons) can be used as a conservative value of expected sensitivities to thermal neutrons for similar muon detectors at future supercolliders. The beta radioactivation of detector walls by thermal neutrons is expected to give a non-negligible contribution into background rate if the fraction of thermal neutrons will be considerably high.

The measured sensitivity of tested detectors to gammas from ^{60}Co source is in order of magnitude higher than sensitivity of these detectors to neutrons. The measured values for Al RDT and CSC are in a good agreement with GEANT simulations where only detector material was taken into account. Because gamma fluence is expected to be approximately in three times lower than neutron fluence [2] the occupancy per one detector channel due to gammas could be higher than due to neutrons. Fortunately the expected spectrum of neutron associated gammas is peaking at the energy about 0.1 MeV and CSC sensitivity expected to be lower for gammas of such energy. So the measured sensitivities to ^{60}Co gammas can be used as a conservative values for the estimations of background

occupancies due to neutron associated gammas.

Bibliography

[1] D. E. Lee, R.E.Prael, L.Waters "Progress Report: Neutron Flux in the GEM Detector" GEM TN-92-91

[2] GEM TDR, GEM TN-93-262

[3] J.F.Briemeister "MCNP: A General Monte Carlo Code for Neutron and Photon Transport" LA-7396-M, Rev.2 Manual UC-32, 1986

[4] R.Brun et al. "GEANT3 User's Guide" CERN-DD/EE 84-1, 1986; "GEANT 3.15, GEANT User's Guide" Revised July 13, 1992

[5] T.A.Gabriel,J.D.Amburgey,B.L.Bishop "CALOR: A Monte Carlo Program Package for Design and Analysis of Calorimeter Systems" ORNL/TM-5619, 1977

[6] A. Korytov, K. Linder, L.S. Osborne, F.E. Taylor "Neutron Sensitivity of LSDT Chambers" GEM TN-92-133

[7] S.Whitaker et al., "The GEM Muon System Based on Cathode Strip Chambers" GEM TN-92-199

[8] D.I.Garber, R.R.Kinsey "Neutron Cross Sections" BNL-325, 1976

[9] P.G.Roll, F.E.Steigert "Effective Charge of Heavy Ions in Various Media" Phys.ReV. v.120, p.470, 1960

Figure captions

Fig.1 Expected spectrum of background neutrons for GEM muon system.

Fig.2 Expected spectrum of background gammas for GEM muon system.

Fig.3 Experimental layout.

Fig.4 Calculated neutron spectrum for set-up with ^{252}Cf source with moderator and 108 mm thick Pb shield.

Fig.5 Cross-section of neutron absorption by Cd nucleus as a function of neutron energy.

Fig.6 Flux of neutrons with energies higher than 0.4 eV behind the Pb shield as a function of R^{-2} where R is the distance between source and neutron counter.

Fig.7 Count rate of RDT as a function of R^{-2} for set-up with a) ^{252}Cf and b) ^{60}Co sources.

Fig.8 RDT count rate after albedo subtraction as a function of thickness of Pb shield between the source and the detector.

Fig.9 Efficiency of fast neutron detection by RDT as a function of iC_4H_{10} in iC_4H_{10}/Ar mixture.

Fig.10 Differential (a) and integrated (b) distributions over collected charge for fast neutron detection by mylar RDT filled with CF_4.

Fig.11 The same as Fig.10 but for thermal neutrons.

Fig.12 The count rate of Al RDT (a) and CSC (b) as a function of delay time after 1 hour of irradiation in thermal neutron flux.

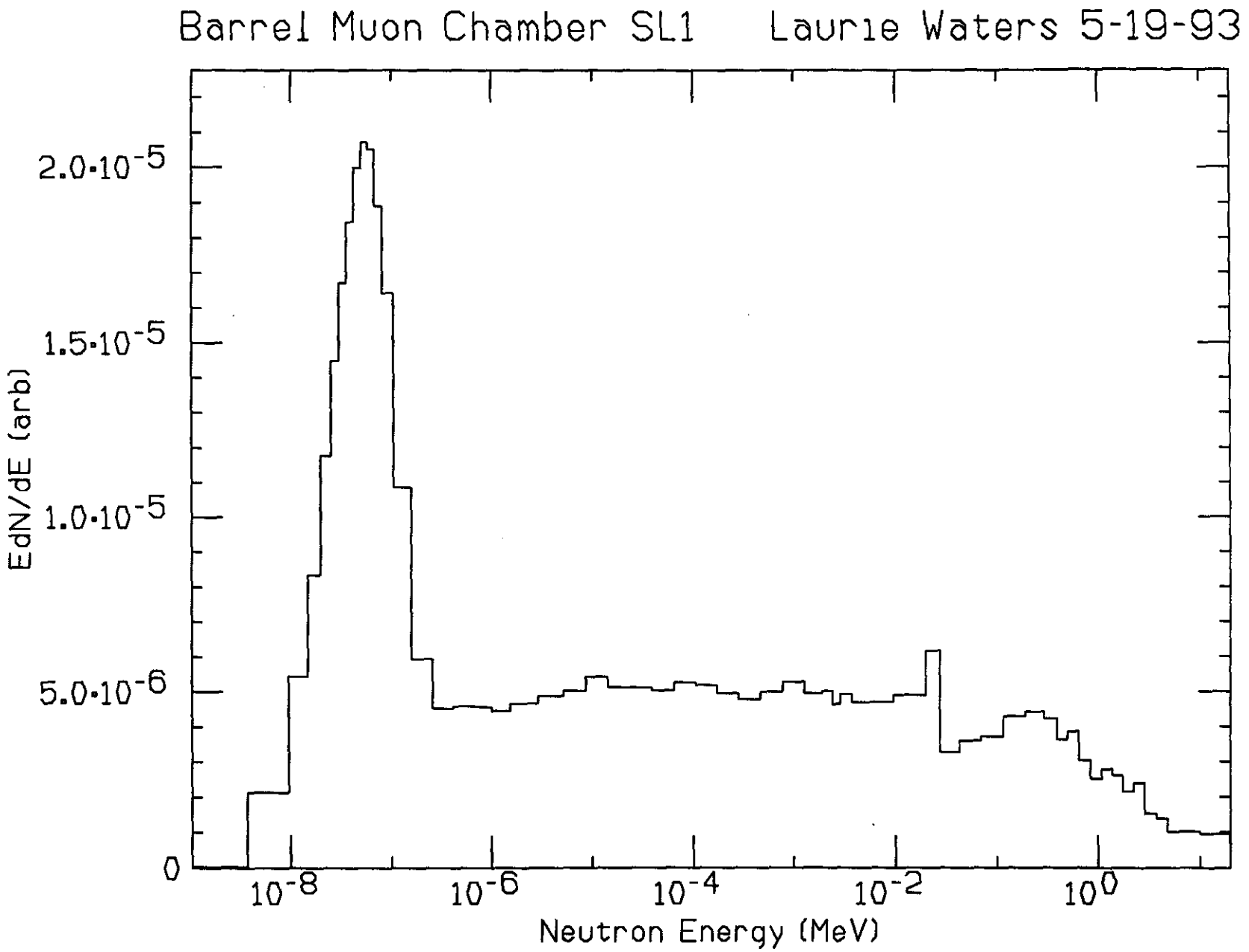
Barrel Muon Chamber SL1 Laurie Waters 5-19-93
2.0·10-5
1.5·10-5
1.0·10-5
5.0·10-6
0
EdN/dE (arb)
10-8
10-6
10-4
10-2
100
Neutron Energy (MeV)

Fig. 1

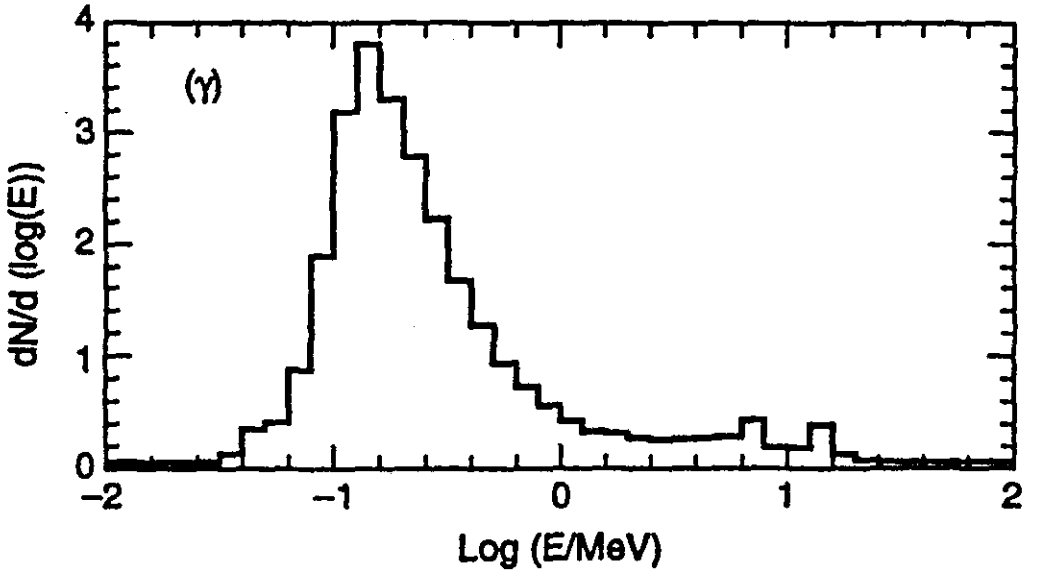

Fig. 2

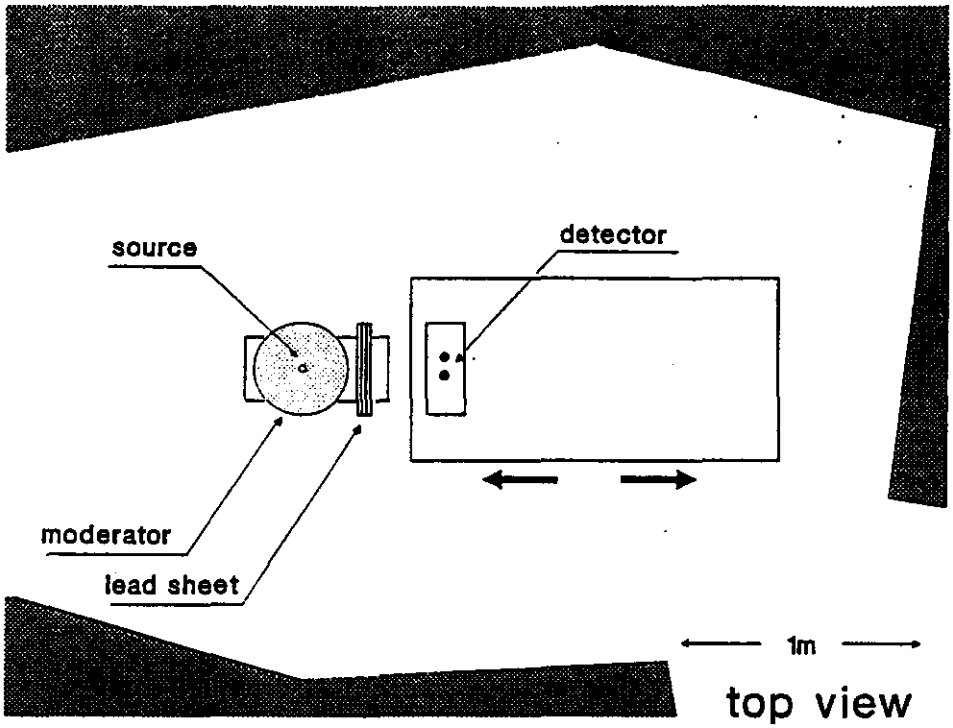
source
detector
moderator
lead sheet
1m
top view

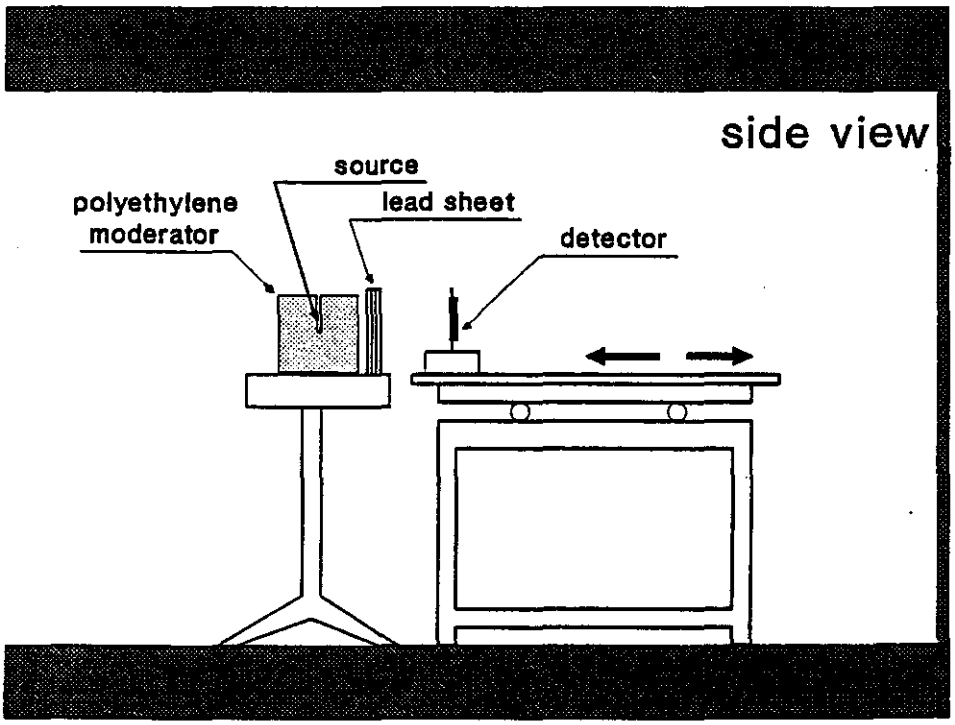
side view
source
polyethylene moderator
lead sheet
detector

Fig.3

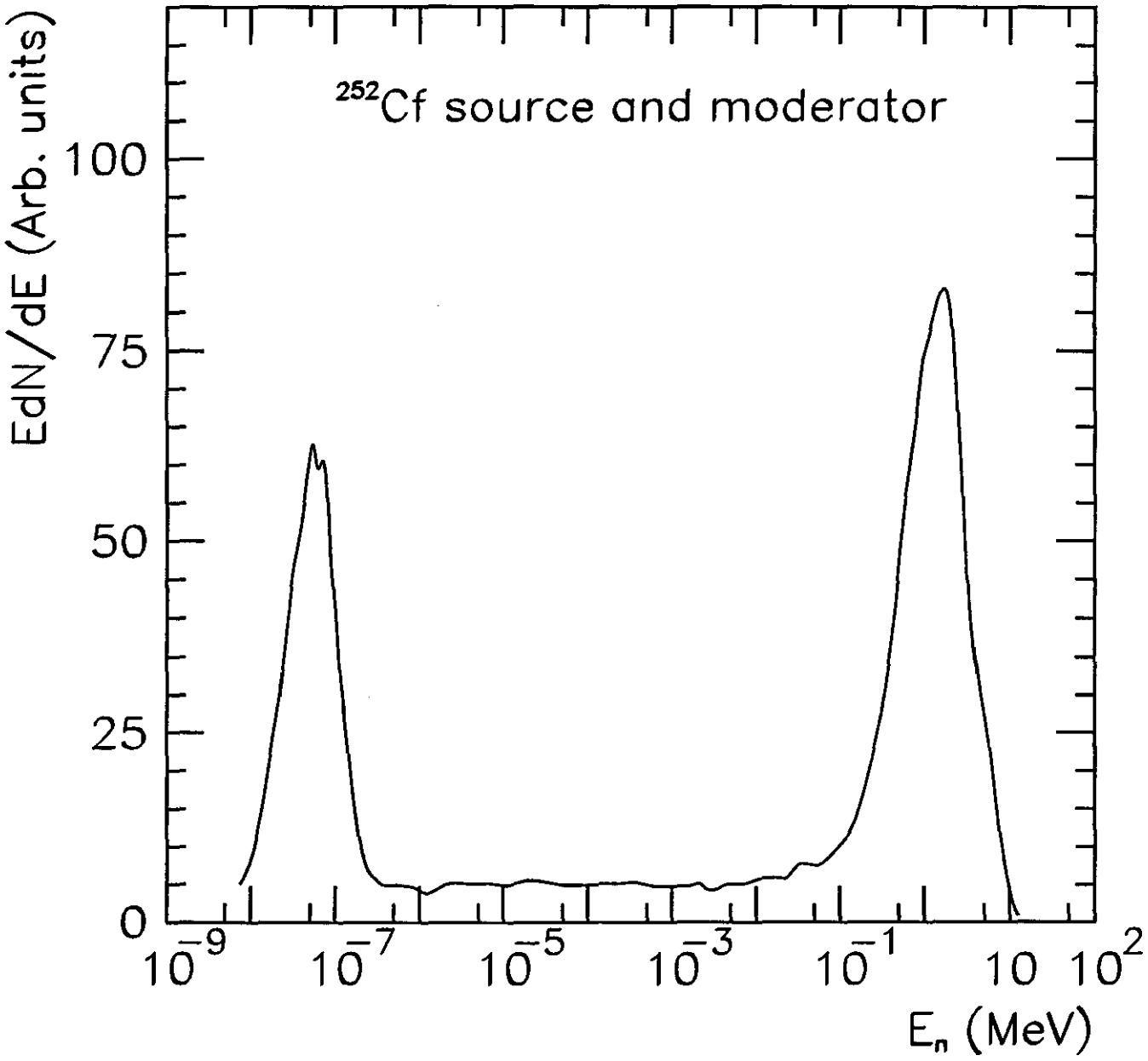
^{252}Cf source and moderator
EdN/dE (Arb. units)
100
75
50
25
0
10^{-9}
10^{-7}
10^{-5}
10^{-3}
10^{-1}
10
10^{2}
E_n (MeV)

Fig.4

$_{48}Cd$

σ_{tot}

[1281]

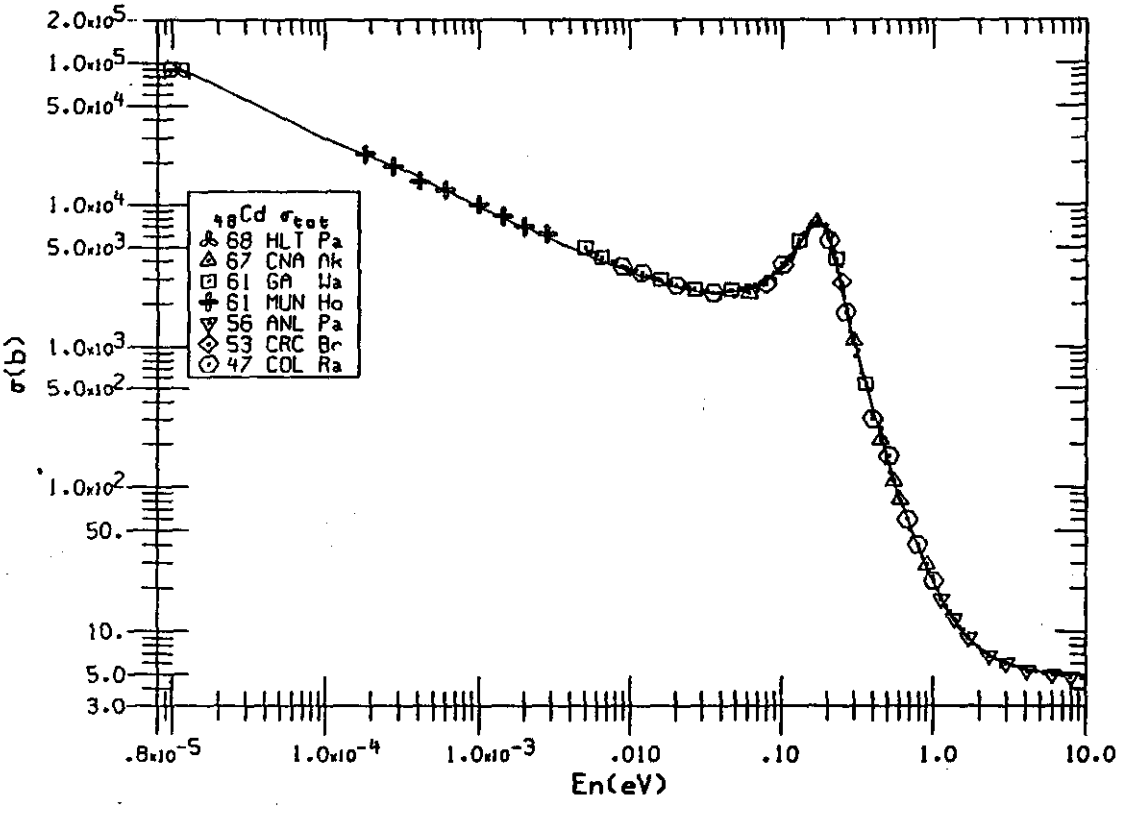

Fig.5

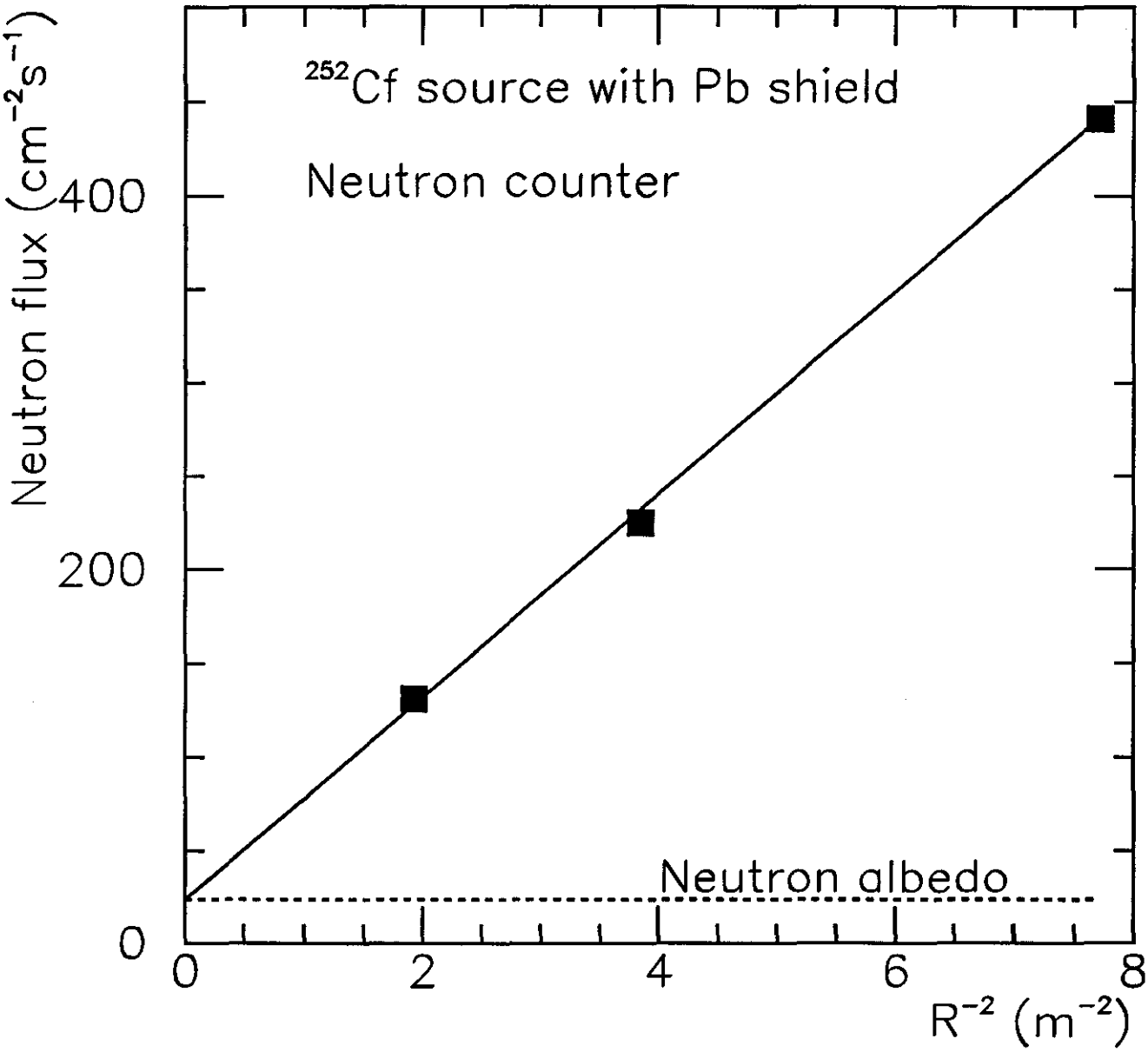
^{252}Cf source with Pb shield
Neutron counter
Neutron albedo
Neutron flux (cm^{-2}s^{-1})
400
200
0
0
2
4
6
8
R^{-2} (m^{-2})

Fig.6

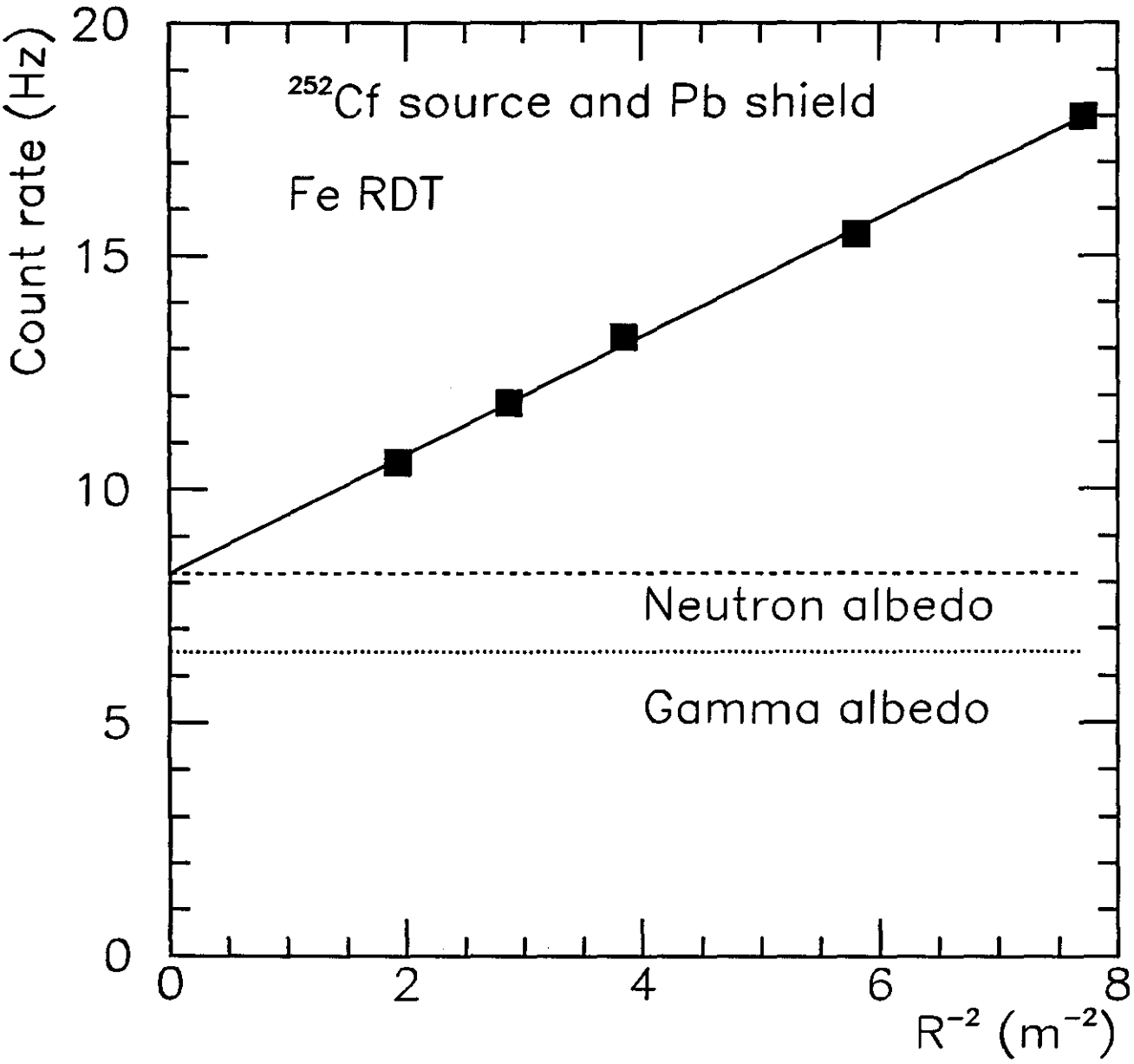
Count rate (Hz)
20
15
10
5
0
^{252}Cf source and Pb shield
Fe RDT
Neutron albedo
Gamma albedo
0
2
4
6
8
R^{-2} (m^{-2})

Fig. 7a

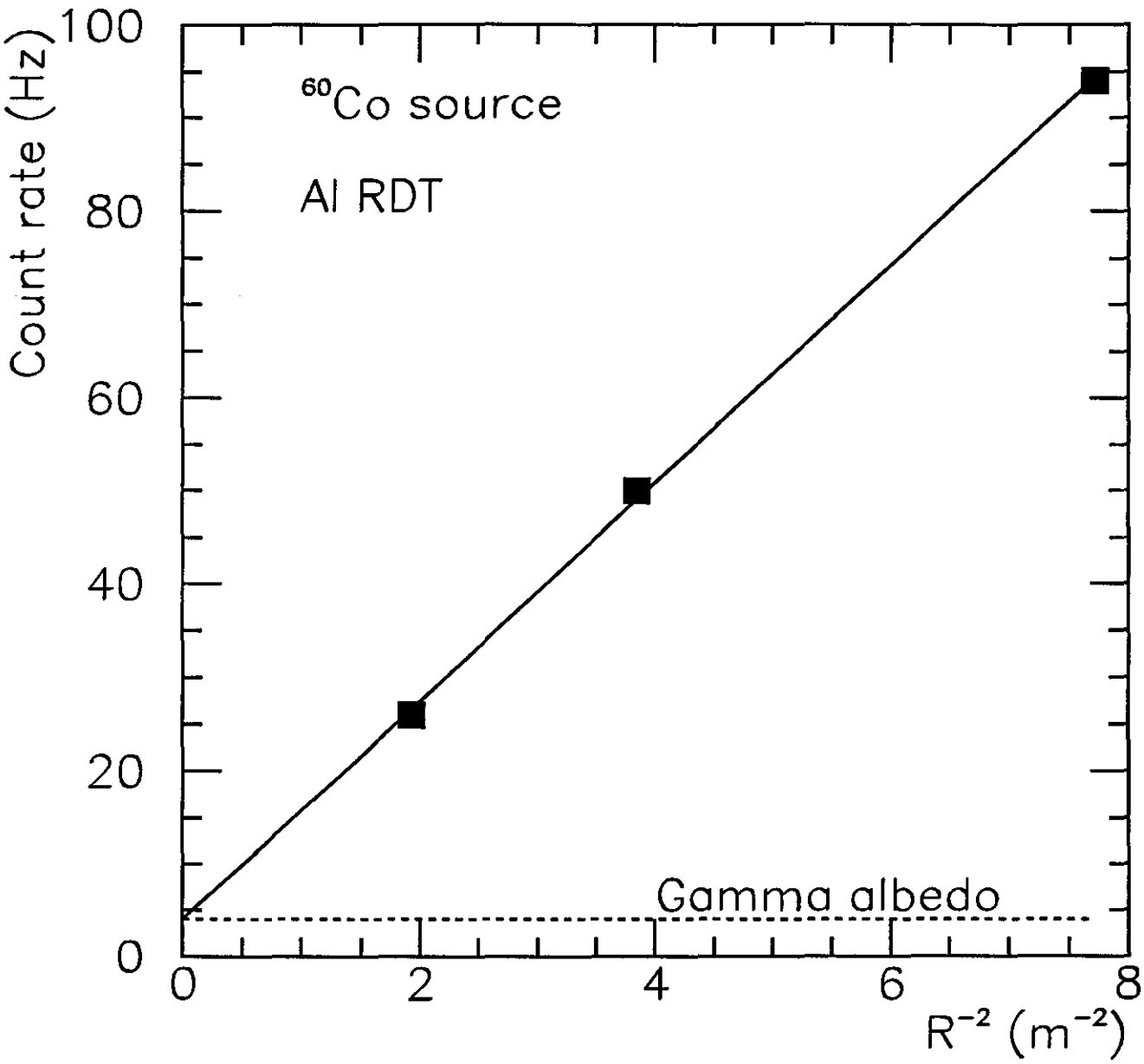
Count rate (Hz)
100
80
60
40
20
0
^{60}Co source
Al RDT
Gamma albedo
0
2
4
6
8
R^{-2} (m^{-2})

Fig. 7b

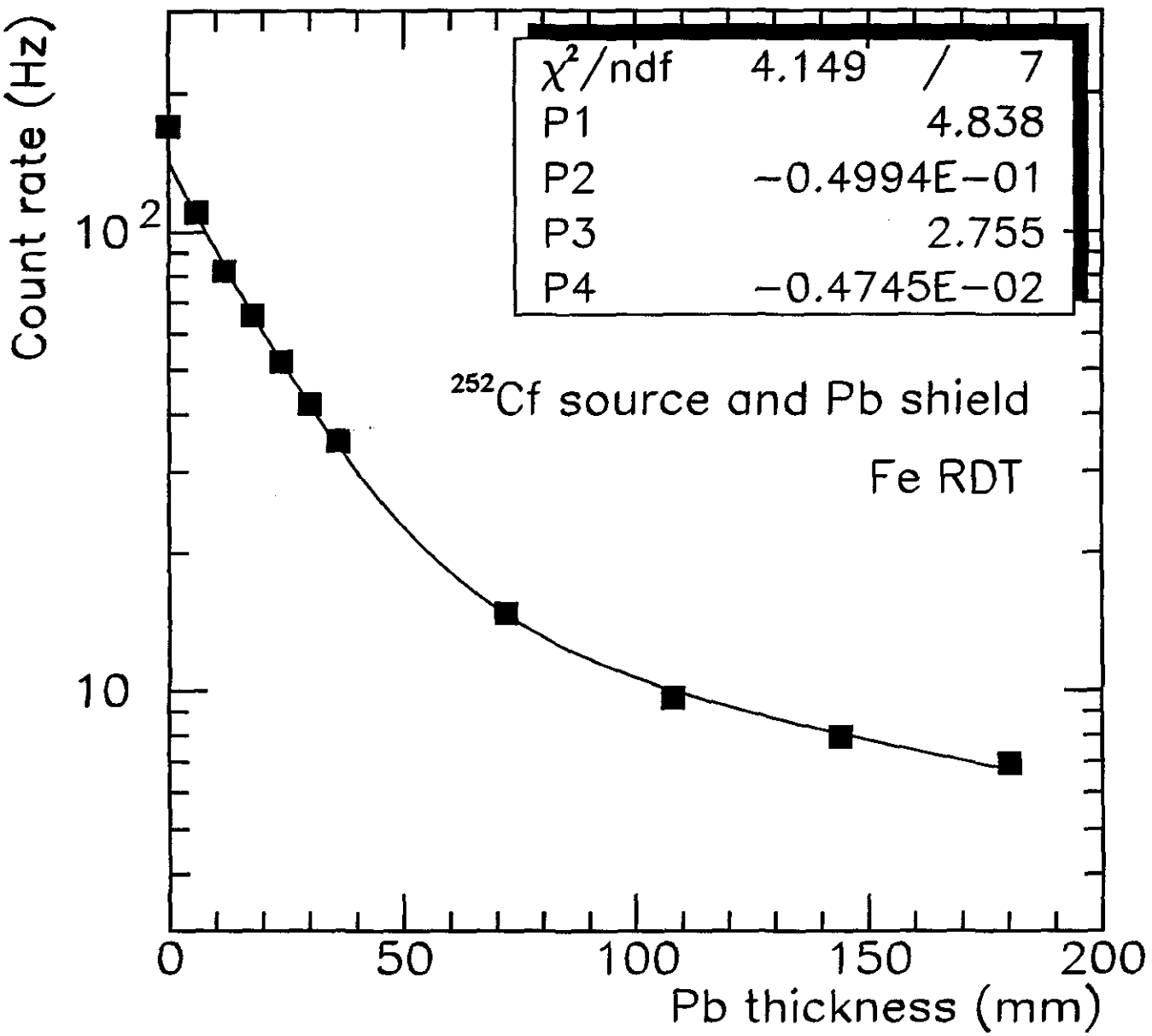
Count rate (Hz)
10^2
10
0
50
100
150
200
Pb thickness (mm)
χ^2/ndf 4.149 / 7
P1 4.838
P2 −0.4994E−01
P3 2.755
P4 −0.4745E−02
^{252}Cf source and Pb shield
Fe RDT

Fig. 8

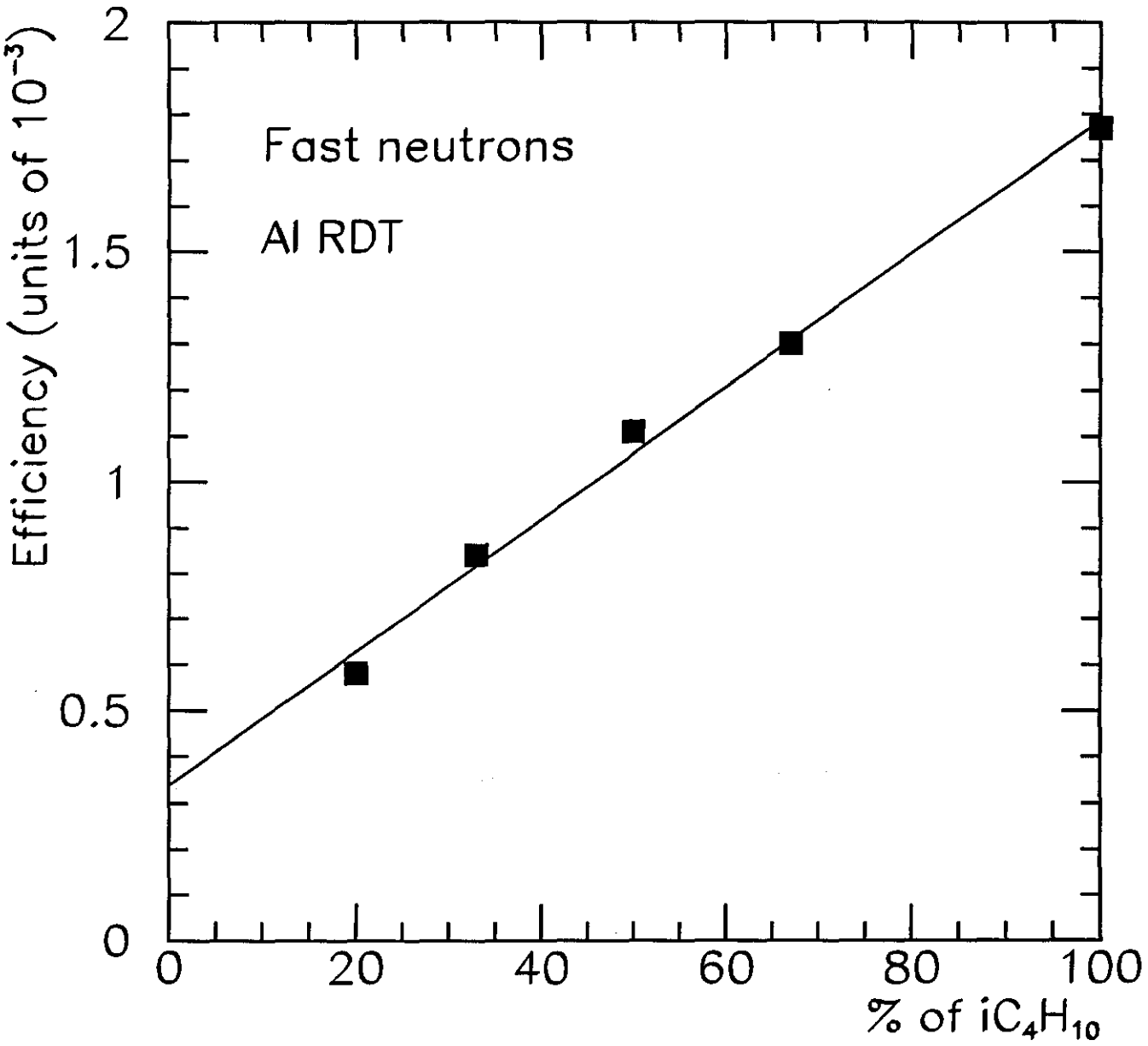
Efficiency (units of 10^{-3})
2
1.5
1
0.5
0
Fast neutrons
Al RDT
0
20
40
60
80
100
% of iC_4H_{10}

Fig.9

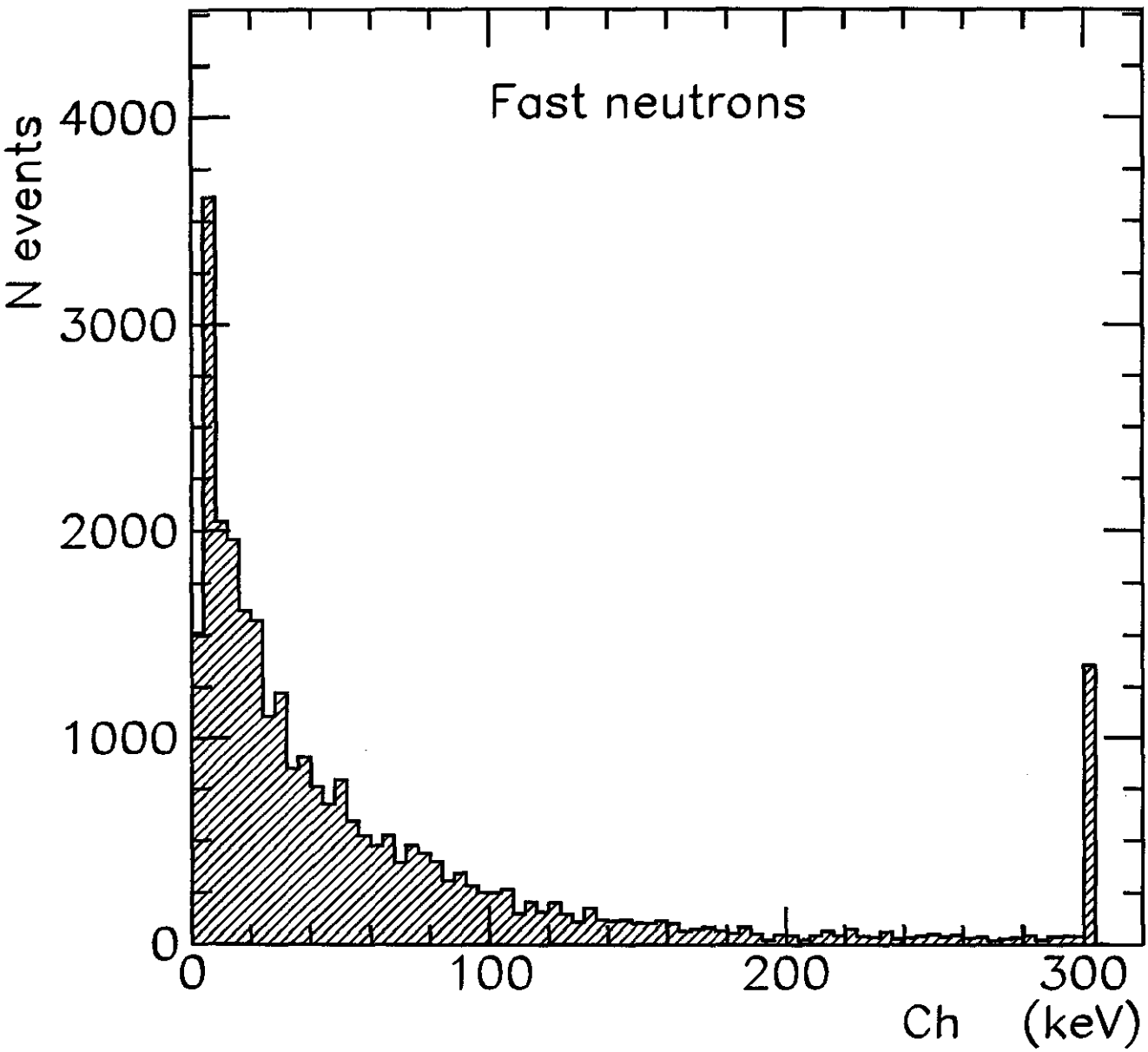
Fast neutrons
N events
4000
3000
2000
1000
0
0
100
200
300
Ch (keV)

Fig. 10a

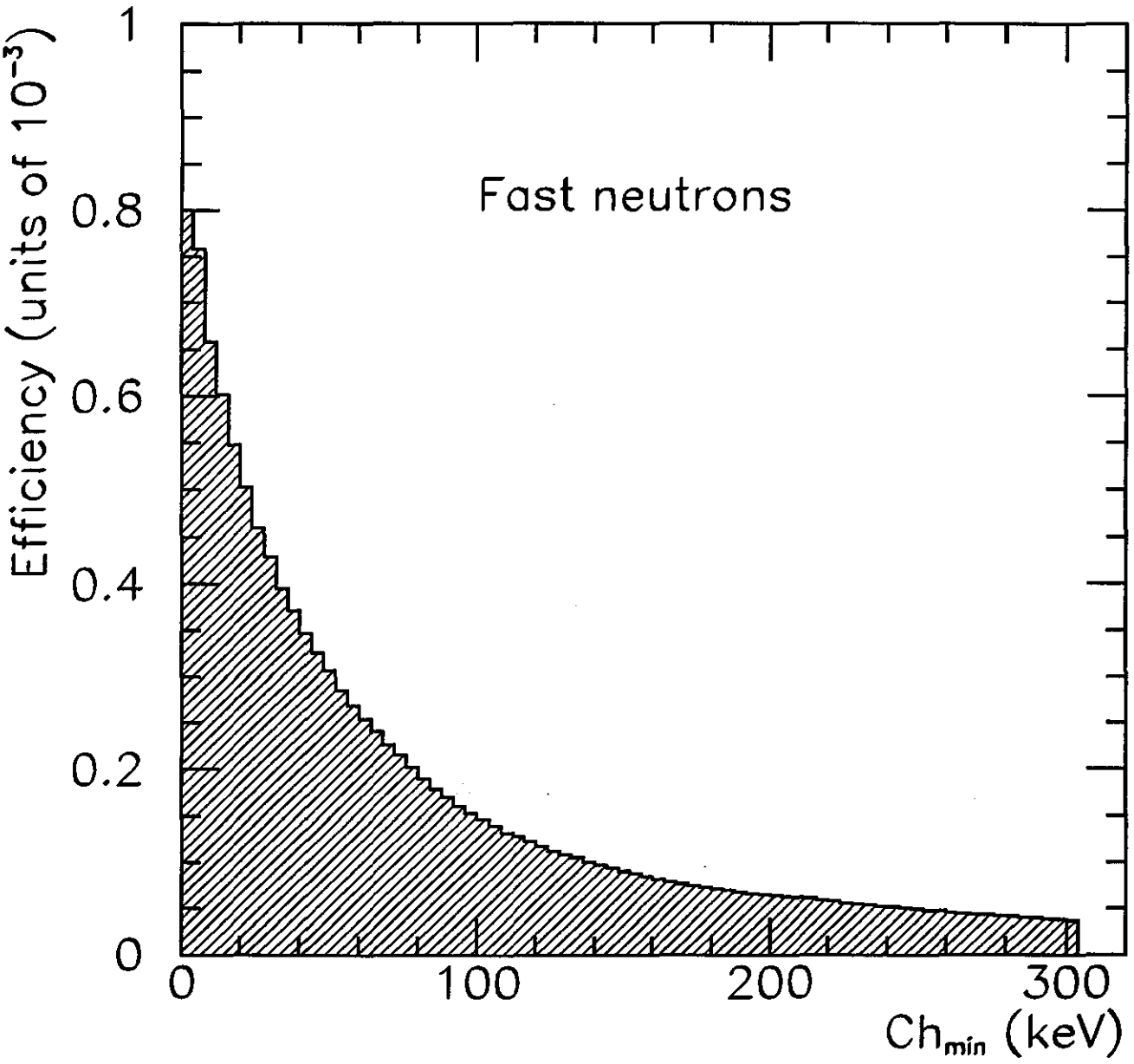
Fast neutrons
Efficiency (units of 10^{-3})
1
0.8
0.6
0.4
0.2
0
0
100
200
300
Ch_{min} (keV)

Fig. 106

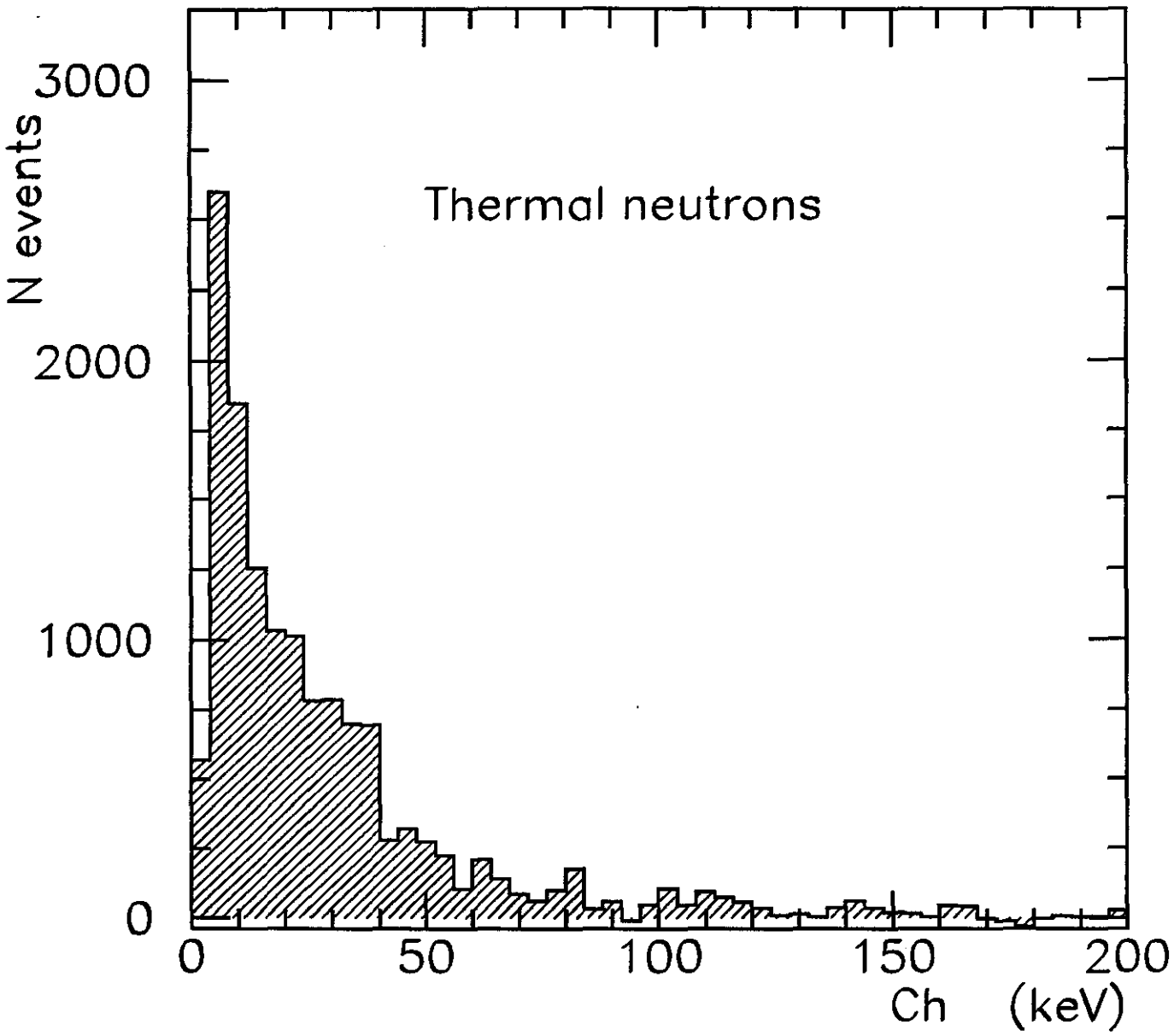
Thermal neutrons
N events
3000
2000
1000
0
0
50
100
150
200
Ch (keV)

Fig. 11a

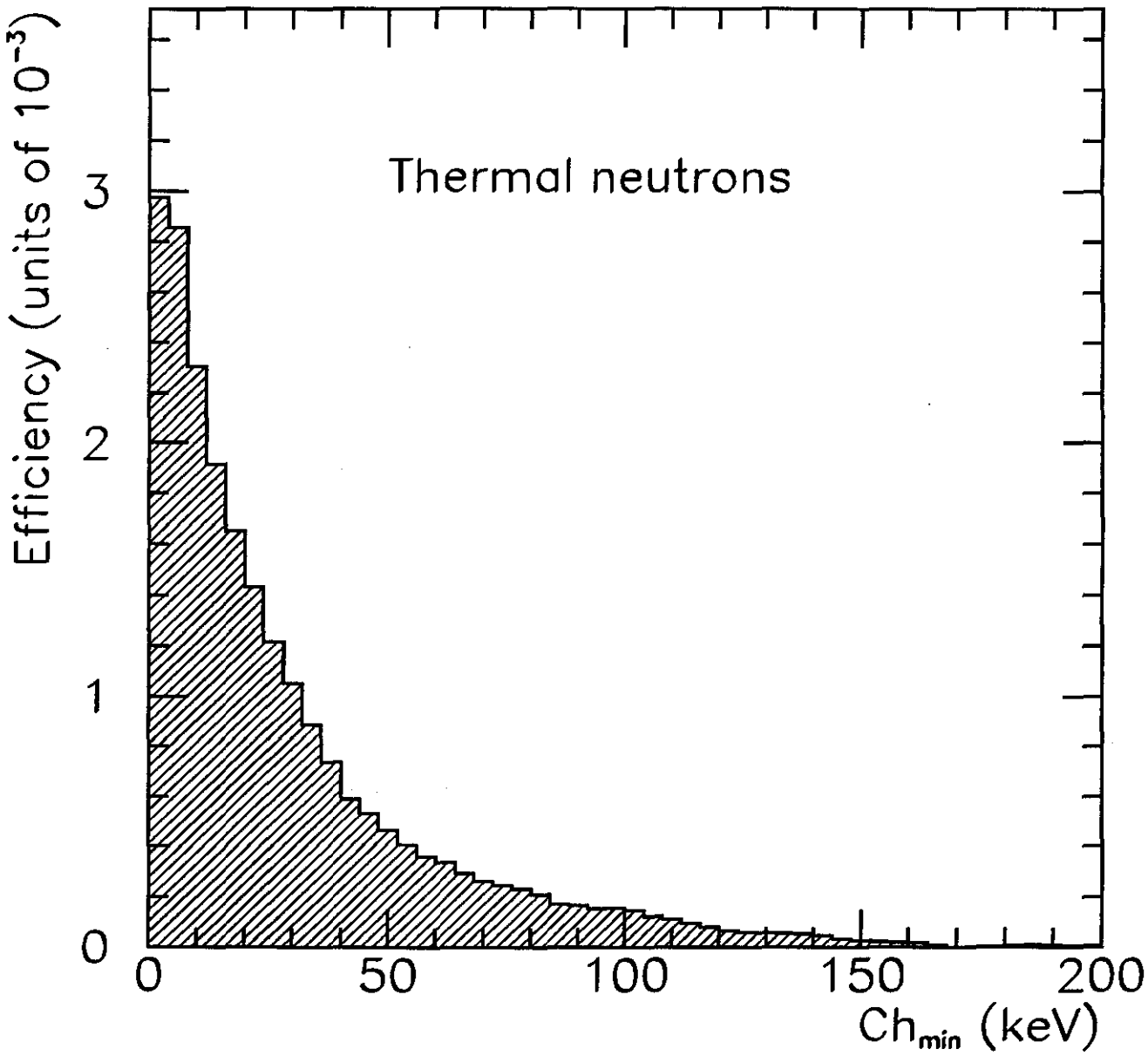
Thermal neutrons
Efficiency (units of 10^{-3})
0
1
2
3
0
50
100
150
200
Ch_{min} (keV)

Fig. 11b

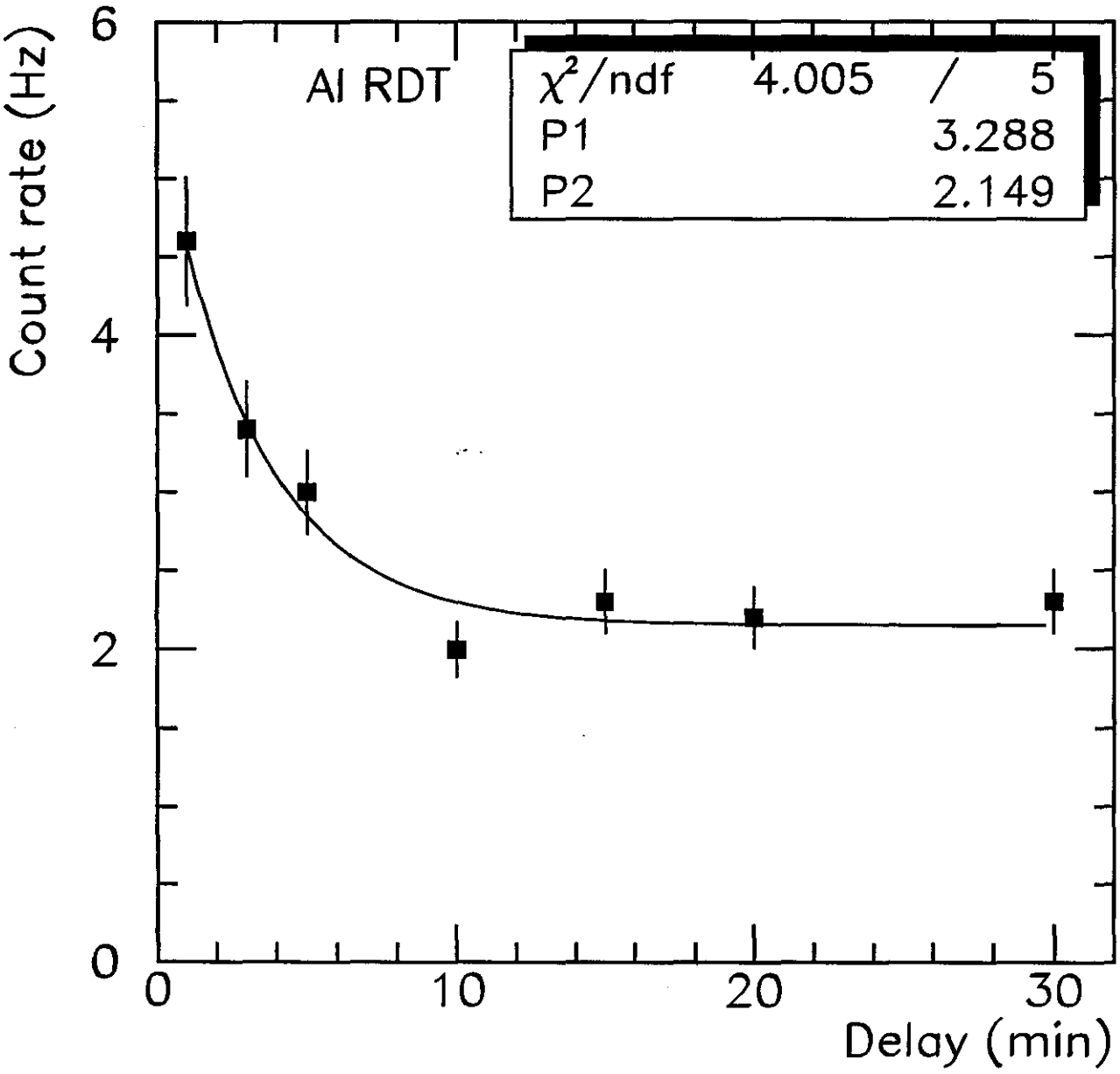
Al RDT
χ²/ndf 4.005 / 5
P1 3.288
P2 2.149
Count rate (Hz)
Delay (min)
0
2
4
6
0
10
20
30

Fig. 12a

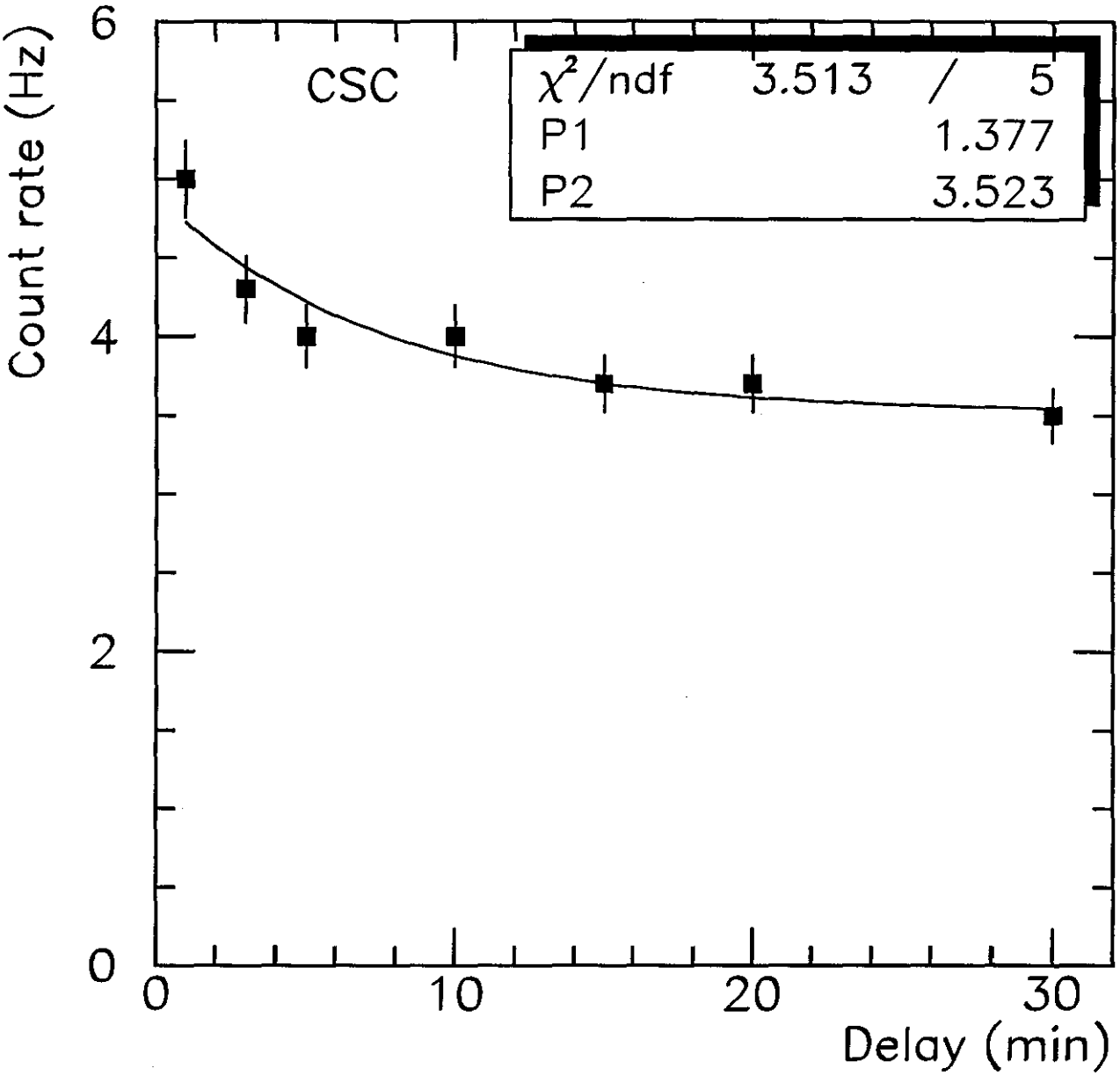
CSC
χ^2/ndf 3.513 / 5
P1 1.377
P2 3.523
Count rate (Hz)
Delay (min)
0
2
4
6
0
10
20
30

Fig. 126